Theoretical Chemistry Accounts (2020) 139:182
https://doi.org/10.1007/s00214-020-02695-9

REGULAR ARTICLE

Kinetics theoretical study of the $O(^3P) + C_2H_6$ reaction on an *ab initio*-based global potential energy surface

M. Garcia-Chamorro[1] · J. C. Corchado[1] · J. Espinosa-Garcia[1]

Received: 8 October 2020 / Accepted: 11 November 2020 / Published online: 23 November 2020

Abstract
Based on a recently developed analytical full-dimensional potential energy surface describing the gas-phase $O(^3P) + C_2H_6$ reaction (Espinosa-Garcia et al. in Phys Chem Chem Phys 22:22,591, 2020), thermal rate constants and kinetic isotope effects (KIEs) were studied in the temperature range 200–3000 K using three different kinetics tools: variational transition-state theory with multidimensional tunnelling corrections (VTST/MT), ring polymer molecular dynamics (RPMD), and quasi-classical trajectory (QCT) calculations. Except the last method, which failed in the description at low temperatures, as was expected due to its classical nature, the other two methods present rate constants with differences between them of 3% at low temperatures and 25% at high temperatures, simulate the experimental measurements in the intermediate temperature range, 500–1000 K, and are intermediate between two reviews of experimental measurements at low and high temperatures, where the experimental evidence shows differences of a factor of about 5. This result shows that both methods capture quantum effects, such as zero-point energy, tunnelling, and recrossing effects. The kinetics of the title reaction presents a non-Arrhenius behavior, where the activation energy increases with temperature. Two KIEs were analyzed. For the H/D isotopes, the KIE decreases with temperature, from 46.55 to 1.18 in the temperature range 200–3000 K, while the $^{12}C/^{13}C$ KIE presents values close to unity. Unfortunately, no experimental information is available for comparison.

Keywords Theoretical kinetics · Polyatomic reactions · Potential energy surface · Comparison of kinetic theories, thermal rate constants · Kinetic isotope effects

1 Introduction

Interest in the kinetics study of the title reaction is threefold: firstly, for its importance in combustion chemistry [1], secondly, due to the large uncertainties of the experimental values at low and high temperatures [2], and thirdly, as a severe test of the recently developed full-dimensional analytical potential energy surface, PES-2020 [3]. Although experimentally this reaction has been widely studied since 1962 (an exhaustive review can be found in the NIST kinetics database [2]), the theoretical studies are scarce [4–7] and, in general, low-level computational tools were used. Experimentally, the widest temperature range reviews were presented by Tsang and Hampson [8] on the temperature range 300–2500 K and by Cohen and Westberg [9] on the temperature range 298–3000 K. The first authors proposed the following expression of the rate constant (cm^3 $molecule^{-1}$ s^{-1})

$$k(T) = 6.09\times10^{-11}(\mathrm{T}/298\ \mathrm{K})^{0.60}\mathrm{e}^{-30.60[\mathrm{kJ/mol}]/\mathrm{RT}}(300-2500\ \mathrm{K}) \quad (1)$$

with uncertainty 2.0, while the second authors gave

$$k(T) = 2.21\times10^{-15}(\mathrm{T}/298\ \mathrm{K})^{6.50}\mathrm{e}^{-1.16[\mathrm{kJ/mol}]/\mathrm{RT}}(298-1300\ \mathrm{K}) \quad (2)$$

and

$$k(T) = 4.32\times10^{-9}\mathrm{e}^{-58.28[\mathrm{kJ/mol}]/\mathrm{RT}}(1300-3000\ \mathrm{K}) \quad (3)$$

with uncertainty 2.51. Both reviews present good agreement in the intermediate temperature range, 500–1000 K, but they differ by a factor of about 5 at low and high temperatures. For instance, at 300 K, both reviews give rate constant values of 2.88×10^{-16} and 1.45×10^{-15}, respectively, while at 2500 K, the values are 5.01×10^{-11} and 2.61×10^{-10}. Theoretically, the first kinetics studies were performed by Mayer

✉ J. Espinosa-Garcia
joaquin@unex.es

[1] Departamento de Química Física and Instituto de Computación Científica Avanzada, Universidad de Extremadura, 06071 Badajoz, Spain

and Schieler in 1968 [4]. Mahmud et al. [5] performed transition-state theory (TST) studies where the tunnelling factor was included by using the Eckart approach. Later, Troya [6] based on *ab initio* calculations of low level (optimized geometries at the MP2 level) used the TST method with the naïve Wigner approach to simulate the tunnelling effect, obtaining a rate constant at 298 K which underestimates the experimental evidence. In this study, no variation of the rate constant with temperature was performed. Finally, Huynh et al. [7] used variational TST and small curvature tunnelling approaches to estimate the rate constants in the temperature range 300–3000 K. In general, agreement with experiment is reasonable or good, which is surprising given the low-level electronic structure calculations used in the description of the potential energy surface, PES.

In order to improve the previous theoretical description of the title reaction, in the present theoretical kinetics study, we used the following theoretical tools. The PES-2020 surface, which is an analytical full-dimensional potential energy surface recently developed in our group [3], where high-level *ab initio* calculations were used as input data. Based on this surface, three kinetics approaches were used: variational transition-state theory with multidimensional tunnelling correction, VTST/MT; ring polymer molecular dynamics, RPMD; and quasi-classical trajectory (QCT) calculations. The reaction of oxygen atoms with ethane is practically thermoneutral, $\Delta H_r\,(^\circ K) = -2.33$ kcal mol^{-1}, and presents a noticeable reaction barrier, 10.70 kcal mol^{-1} [3]. Consequently, the rate constants will be low or very low at low temperatures, $T < 500$ K, and in this temperature regime, the quantum mechanics tunnelling correction will be very important. Given the experimental uncertainties previously noted, our main aims were first to analyze different effects, such as zero-point energy (ZPE), tunnelling and recrossing, which affect thermal rate constants; and, second, since quantum-mechanical methods for full-dimensional polyatomic systems (in this case nine atoms) are practically forbidden today, to test the three kinetics approaches.

The paper is organized as follows. Section 2 is devoted to the detailed description of the theoretical tools used: VTST/MT, RPMD and QCT theories based on the PES-2020 surface. In Sects. 3 and 4, the kinetics results are analyzed and discussed, and compared with the experimental evidence when available. Finally, the conclusions are summarized in Sect. 5.

2 Theoretical tools

We chose these three theories, VTST/MT, RPMD, and QCT, because they are affordable enough to be employed in a system of the size of the present system and to face the kinetic problem from different perspectives using different approaches. The VTST/MT method is based on the transition-state theory and the tunnelling transmission coefficient is included as a factor. This method incorporates recrossing effects by minimizing the generalized transition-state theory rate constants, $k^{GT}(T, s^*)$, or equivalently by calculating the maximum of the free energy, $\Delta G(T, s^*)$, which is obtained at each temperature T by varying the dividing surface between reactants and products, s^*. The location of the dividing surface is strongly dependent on the treatment of the anharmonicity of the lowest vibrational frequencies in the zone of the saddle point, of the mode-mode coupling or of the consideration of the reaction coordinate as separable motion, this location being the main disadvantage of this approach. In its canonical version, CVT, the rate constant expression is given by,

$$k^{CVT}(T) = \sigma \frac{k_B T}{h} K^o \min_s \exp\left[\frac{-\Delta G^{GT,o}\left(T, s^{*,CVT}\right)}{k_B T}\right] \quad (4)$$

where σ, K^o, k_B and h mean the symmetry factor (6 equivalent hydrogen atoms for the forward reaction), the reciprocal of the standard-state concentration (1 molecule cm^3), the Boltzmann constant and the Planck constant, respectively. As noted, we have obtained the symmetry number, σ, from the number of equivalent hydrogen atoms, $\sigma = 6$ in this case. A more rigorous justification of this factor is obtained from the number of rotational symmetry operations of both reactants and transition state [10]. So, the symmetry number is given by

$$\sigma = \frac{\sigma_{rot,\,R}}{\sigma_{rot,TS}} = \frac{\sigma_{oxygen}\,\sigma_{rot,ethane}}{\sigma_{rot,TS}} = \frac{1.6}{1} = 6 \quad (5)$$

where ethane, both staggered (D_{3d} symmetry) or eclipsed (D_{3h} symmetry) conformations, presents a rotational symmetry number $\sigma_{rot,ethane} = 6$, while the transition state with C_s symmetry, presents $\sigma_{rot,TS} = 1$. This results agrees with the intuitive argument of the number of equivalent hydrogen atoms.

The tunneling transmission coefficient is incorporated by using the microcanonical optimized multidimensional tunnelling approach, μOMT [11], which is, at each energy, the largest of the tunnelling probabilities using the approaches of small and large curvature, SCT and LCT. This approach is used because the title reaction presents a heavy–light–heavy mass combination and, therefore, an important tunneling contribution at low temperatures is expected. In these kinetics calculations, the Polyrate-2016 code [12] was used in the temperature range 200–3000 K.

The RPMD theory is based on the so-called classical isomorphism, where a quantum system is described by a classical ring polymer composed of n beads or copies of the original system, which are inter-connected by harmonic

springs [13]. The rate constant expression is given as the product of two factors,

$$k_{\mathrm{RPMD}}(T) = k_{\mathrm{QTST}}\left(T, \xi^{\neq}\right) \cdot \kappa(t \to \infty, \xi) \tag{6}$$

where k_{QTST} $(T, \xi^{\neq})$ is a static term at temperature T at the reaction coordinate $\xi^{\neq}$, which corresponds to the centroid-density quantum transition-state theory rate constant [14–16], and $\kappa(t \to \infty, \xi)$ is a dynamic term corresponding to the ring polymer transmission coefficient. The first factor includes the tunnelling transmission coefficient and is evaluated from the free energy along the reaction coordinate [17], also known as potential of mean force, PMF. The second factor includes the recrossing effects and it ensures that the final rate constant, k_{RPMD} (T), is independent of the locating of the dividing surface along the reaction path, which was a disadvantage in the TST-based approaches. In this case, the kinetic calculations were performed using the RPMD code [17]. While the RPMD theory is exact in the regime of high temperatures where the recrossing effects play the most important role [18–24], the main disadvantage is the description of low temperatures where the tunnelling effect is more important, with differences by a factor 2–4 from exact quantum mechanical calculations [25]. Due to the very expensive computational cost, only the following temperatures were analyzed: 300, 500, 1000, 1500 and 2000 K, which cover the temperature range of interest for this study. Table 1 lists the parameters used in the RPMD calculations, and Figs. 1 and 2 show, respectively, the potential mean force and the recrossing effects, at each temperature.

Finally, the QCT theory follows a different approach by using quasi-classical trajectory calculations in the estimation of the rate constants, starting from the reaction cross section at temperature T, σ_r (T),

$$k(T) = \left(\frac{8k_B T}{\pi \mu}\right)^{1/2} \sigma_r(T) \tag{7}$$

where μ is the reduced mass and σ_r (T) is given by

$$\sigma_r = \pi . b_{\mathrm{max}}^2 N_r / N_T \tag{8}$$

b_{max}, N_r and N_T being, respectively, the maximum impact parameter, the number of reactive trajectories and the number total of trajectories run. Two important limitations of this theory, given its classical nature, are the non-consideration of tunnelling corrections and the zero-point energy (ZPE) violation problem, i.e., the incorrect consideration of reactive trajectories where the products of reaction appear with vibrational energy below their respective ZPEs. In order to minimize this defect a passive method, DZPE (double ZPE) was used [26–30], where we only considered reactive trajectories in which each product, OH and C_2H_5, presented a vibrational energy above its ZPE. All dynamics calculations were performed by using the VENUS code [31, 32] at 300, 500, 1000, 1500 and 2000 K. At each temperature, 500 000 trajectories were run with an initial and final separation C–O distance of 15 Å and a propagation step of 0.1 fs. The translational, rotational and vibrational energies of reactants were selected by thermal sampling at each temperature, where the maximum impact parameters were, respectively, 1.5, 2.0, 3.0, 3.1 and 3.4 Å.

The entire kinetics study was performed on an *ab initio*-based analytical full-dimensional potential energy surface, named PES-2020, recently developed in our group [3]. In brief, this is a valence bond (VB) augmented with molecular mechanics (MM) functional form, VB/MM, where intuitive chemical concepts were used in its development: stretching, bending and torsional motions. This functional form represents this nine-body system with 21 degrees of freedom, depending on 60 adjustable parameters. These parameters were fitted to high-level *ab initio* calculations, at the CCSD(T)-F12/aug-cc-pVDZ and CCSD(T)-F12/aug-cc-pVTZ explicitly correlated levels. The root-mean-square error (RMSE) is 0.84 kcal mol^{-1}, with the largest deviation of 1.50 kcal mol^{-1}. This PES-2020 presents a smooth and continuous change from reactants to products, with an exothermicity of ΔH_r $(0\ K) = -2.33$ kcal mol^{-1}, reproducing the experimental information obtained from the corresponding enthalpies of formation of reactants and products, and a barrier height of 10.70 kcal mol^{-1}, reproducing the high level *ab initio* information [3]. In addition, the title reaction presents an additional difficulty related with the presence of two surfaces (^{3}A′ and ^{3}A″ for a collinear approach with symmetry C_{3v}) associated to the spin-orbit splitting of the O(^{3}P) reactant. These surfaces correspond to different orientations of the half-filled p-orbital of the oxygen atom relative to the plane containing a C–H bond. In our previous paper [3], we noted that both surfaces present similar barrier heights and because the transition-state structure for the title reaction belongs to the C_s point group, both have the same A symmetry. PES-2020, therefore, represents the hydrogen abstraction reaction of the title reaction on the lowest-energy triplet surface. Based on this surface, in a previous paper [3] dynamics calculations were performed using quasi-classical trajectory calculations at different collision energies, and it was found that the largest fraction of the available energy was deposited as translational energy, with a scattering distribution evolving from backward to forward when collision energy increases. Finally, cold rotational and vibrational distributions of the OH(v, j) product were obtained, reproducing the experimental evidence [33–35]. This finding is very interesting because previous theoretical calculations [36] failed in the roto-vibrational description. These results give confidence to the accuracy of the new PES-2020,

Table 1 Input parameters for the RPMD rate calculations on the $O(^3P)+C_2H_6$ reaction

Parameter	$O(^3P)+C_2H_6 \rightarrow OH+C_2H_5$	Explanation
Command line parameters		
Temp.	300–2000	Temperature (K)
N_{beads}	128 (300 K); 64 (500 K) 16 (1000 K); 8 (1500 K) 8 (2000 K)	Number of beads
Dividing Surface parameters		
R_∞	15	Dividing surface parameter (distance). Angstroms
N_{bond}	1	Number of forming and breaking bonds
$N_{channel}$	6	Number of aquivalent product channels
C	−0.32018900, 0.42710500, −0.2826720	Cartesian coordinates (x, y, z) of the intermediate geometry. (angstroms)
C	−0.09393696, −0.07642951, 1.1149980	
H	0.60951350, 0.39532950, −0.8506564	
H	−1.06112400, −0.19040180, −0.7903324	
H	−0.68033470, 1.45557200, −0.2590688	
H	0.22628480, −1.11852200, 1.1289320	
H	0.61190260, 0.54538160, 1.6661410	
H	−1.14344400, −0.05308237, 1.7967710	
O	−2.10945000, −0.05083060, 2.4841930	
Thermostat	'Andersen'	Thermostat option
Biased sampling parameters		
$N_{windows}$	110	Number of windows
ξ_i	-0.05	Center of the first window
$d\xi$	0.01	Window spacing step
ξ_N	1.05	Center of the last window
dt	0.0001	Time step (ps)
k_i	2.72	Umbrella force constant ((T/K) eV)
$N_{trajectories}$	100	Number of trajectories
$t_{equlibration}$	20	Equilibration period (ps)
$t_{sampling}$	100	Sampling period in each trajectory (ps)
N_i	2×10^8	Total number of sampling points
Potential mean force calculations		
ξ_0	0.0	Start of umbrella integration
$\xi_\ddagger$	300 0.9750 500–0.9851 1000–0.9886 1500–0.9893 2000–0.9889	End of umbrella integration
N_{bins}	5000	Number of bins
Recrossing factor		
dt	0.0001	Time step (ps)
$t_{equlibration}$	20	Equilibration period (ps) in the constrained (parent) traj. (ps)
$N_{totalchild}$	100000	Total number of unconstrained (child) trajectories.
$t_{childsampling}$	2	Sampling increment along the parent trajectory (ps)
N_{child}	100	Number of child trajectories per one initially constrained configuration
t_{child}	0.05	Length of child trajectories (ps)

The explanation of the format of the input file can be found in http://rpmdrate.cyi.ac.cy/

and permit us to be optimistic in its application to kinetics studies.

Finally, note that in all three kinetics approaches used, VTST/MT, RPMD and QCT, the electronic partition function ratio is included in the rate constant expressions as,

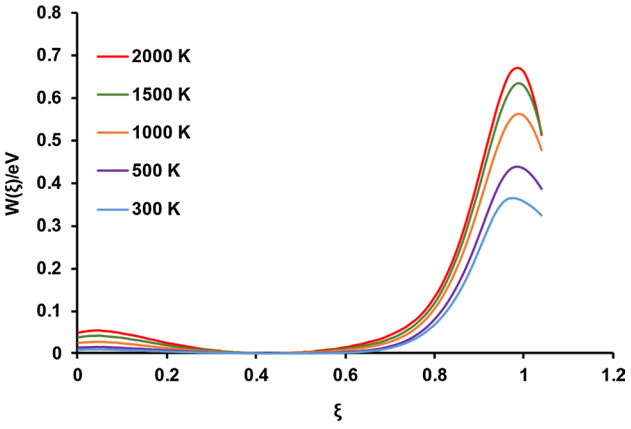

Fig. 1 Ring polymer potentials of mean force (free energy) at 300–2000 K for the $O(^3P)+C_2H_6$ reaction

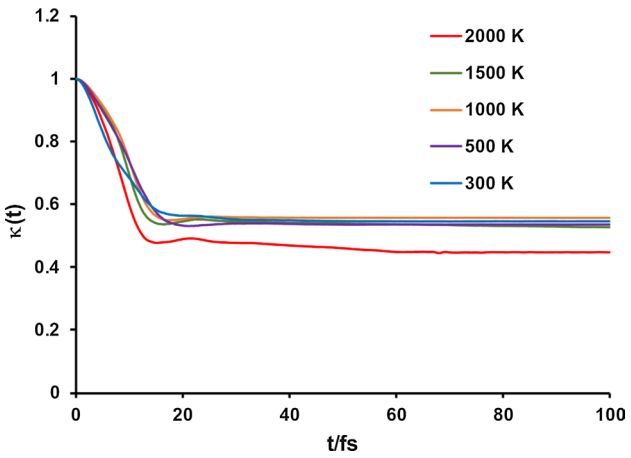

Fig. 2 Ring polymer transmission coefficients at 300–2000 K for the $O(^3P)+C_2H_6$ reaction

$$Q_e(T)=\frac{6}{5+3\exp\left(-E\left(^3P_1\right)/RT\right)+\exp\left(-E\left(^3P_0\right)/RT\right)} \quad (9)$$

where the numerator 6 is a consequence of the triplet state in the transition state and of the presence of the two similar $^3A'$ y $^3A''$ surfaces describing the reactive system [3], $E(^3P_1)$ and $E(^3P_0)$ being the energies of the upper spin–orbit levels of $O(^3P)$ atom relative to its electronic ground state (with values respectively, of 158.29 and 226.99 cm^{-1}). In addition, while VTST/MT and RPMD include the tunnelling effects in their construction, the QCT calculations are classical in nature. So, in this last case and for a direct comparison of methods, the tunnelling factor is included in the rate constant calculation as obtained in the VTST/MT approach using the μOMT method.

3 Rate constant results

As noted in the Introduction, two reviews of experimental measurements [8, 9] have been considered for comparison. These experiments show good agreement in the intermediate temperature zone, 500–1000 K, but they present strong discrepancies at low, 300 K, and high, 2000 K, temperatures, with differences by a factor of about five in both cases. Table 2 lists the rate constants in the temperature range 200–3000 K obtained in the present study by using the CVT/μOMT approach, based on the PES-2020 surface, and Fig. 3 plots the corresponding Arrhenius representation, together with the values from the experimental reviews for comparison. The theoretical CVT/μOMT rates show a non-Arrhenius behavior, with values intermediate between both reviews in the common and wide temperature range 300–2500 K and an excellent agreement in the intermediate zone, 500–1000 K. This result shows that the kinetics tools used (CVT/μOMT + PES-2020) are adequate to study this reaction. By analyzing in more detail this behavior, at low temperatures, when the quantum mechanics tunnelling factor is more important, the present CVT/μOMT method better approaches Cohen-Westberg's review of 1991 [9] (with differences of a factor 1.59 at 300 K), while at high temperatures, where recrossing effects are more important, the present CVT/μOMT rate constants are closer to Tsang-Hampson's review of 1986 [8] (with differences of a factor 1.73 at 2000 K).

In relation to the tunnelling factor at low temperatures, its value varies from 6.33 to 1.02 in the common temperature range 300–2500 K, and even reaches 57.01 at 200 K (temperature not reported in the experiments). This is the expected behavior for a reaction with a high barrier and a heavy–light–heavy mass combination, where reaction path curvature leads to internal centrifugal forces, causing the reactive system to leave the minimum energy path, MEP, and so favouring tunnelling paths on the concave side of the MEP. The non-Arrhenius behavior is a consequence of this strong tunnelling effect. With respect to the recrossing effects, they are defined in the VTST theory as the ratio between CVT(s^*, T) and TST($s=0$, T) rate constants at each temperature, and they measure the effect of the shift from the saddle point ($s=0$) of the maximum of $\Delta G^{GT,o}(s^*, T)$ (Eq. 4). In this theory, this effect is also known as variational effect. The recrossing effect ranges from 0.588 (in $s^*=-0.156$ Å) at 300 K to 0.797 (in $s^*=-0.139$ Å) at 2500 K, i.e., there is a slight shift toward the reactant channel at all temperatures.

Before ending this section, it may be of interest to compare the present VTST/MT rate constants with previous theoretical results, which used lower levels to describe the surface and/or the kinetics [5–7] (Fig. 4). While Troya [6]

Table 2 Rate constants (cm^3 $molecule^{-1}$ s^{-1}) for the $O(^3P) + C_2H_6$ reaction using different theoretical approaches

T(K)	CVT/μOMT	RPMD	QCT-all	QCT-DZPE	Exp-1986[a]	Exp-1991[b]
200	1.44E−17					
250	1.56E−16					
298	8.59E−16					1.38E−15
300	9.14E−16	8.85E−16	3.45E−14	3.45E−14	2.88E−16	1.45E−15
350	3.61E−15					
400	1.09E−14				7.35E−15	1.05E−14
500	5.78E−14	5.65E−14	2.56E−13	3.40E−14	5.29E−14	4.82E−14
600	1.95E−13				2.01E−13	1.65E−13
700	5.00E−13				5.30E−13	4.66E−13
800	1.06E−12				1.11E−12	1.14E−12
900	1.98E−12				1.89E−12	2.49E−12
1000	3.35E−12	3.07E−12	3.39E−12	2.20E−12	3.18E−12	5.02E−12
1500	2.01E−11	1.81E−11	1.24E−11	1.15E−11	1.38E−11	4.03E−11
2000	5.89E−11	4.52E−11	4.37E−11	3.52E−11	3.03E−11	1.30E−10
2500	1.23E−10				5.01E−11	2.61E−10
3000	2.15E−10					4.17E−10

[a]Experimental review from Ref. [8]

[b]Experimental review from Ref. [9]

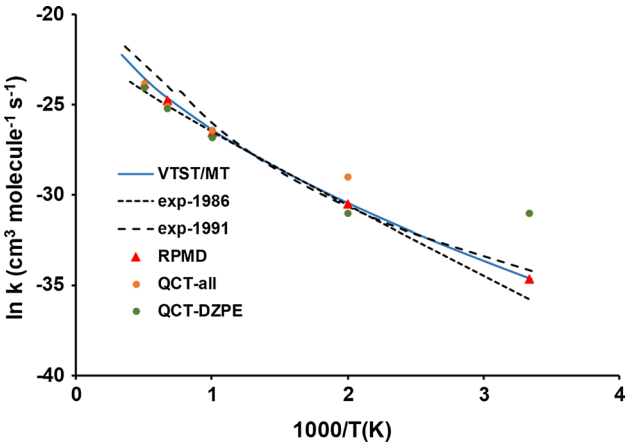

Fig. 3 Arrhenius plots of the rate constants (cm^3 $molecule^{-1}$ s^{-1}) for the title reaction in the temperature range 300–3000 K, using different theoretical kinetics tools and experimental values from the reviews of Refs. [8, 9]. Note that at 300 K the QCT-all and QCT-DZPE rate constants present the same value

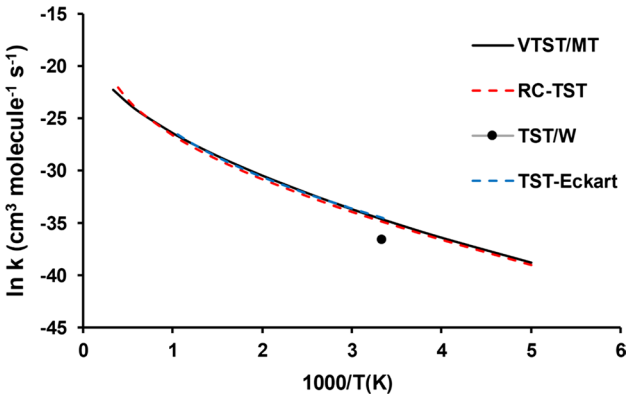

Fig. 4 Arrhenius plots of the rate constants (cm^3 $molecule^{-1}$ s^{-1}) for the title reaction in the temperature range 200–3000 K, from different theoretical kinetics studies. VTST/MT represents the present CVT/μOMT values; TST/Eckart are values from Ref. [5] with Eckart approximation to describe tunnelling; TST/W represents values from Ref. 6 with Wigner approximation to describe tunnelling; RC-TST from Ref. [7] with the SCT approximation to describe tunnelling

reported the rate constant only at 298 K, 1.31 $.10^{-16}$ cm^3 $molecule^{-1}s^{-1}$, by using the TST approach, where the tunnelling effect was included by using the very naïve Wigner method, underestimating the VTST/MT result, two other studies [5, 7] analyzed the variation with temperature. Mahmud et al. [5] analyzed the title reaction based on the transition-state theory where the tunnelling correction was included by the Eckart method, and Huynh et al. [7] used the reaction class TST approach based on density functional theory or semiempirical surfaces. Although both previous studies used kinetics tools (kinetic method + PES) of a lower level than those used in the present work, the agreement is practically quantitative in the wide temperature range 200–3000 K. This excellent agreement can be only possible if an error cancelation is produced in the previous results. For instance, Mahmud et al. [5] gave a barrier height of 12 kcal mol^{-1}, in their empirical estimation, overestimating the more accurate value, 10.70 kcal mol^{-1}, of the PES-2020 surface.

We also analyzed the kinetics of the title reaction by using a different approach, the RPMD theory. The rate constants at selected temperatures, 300, 500, 1000, 1500 and 2000 K,

also appear in Table 2 and Fig. 3. As in the case of the VTST/MT theory, the RPMD rate constants are within the range of the two experimental reviews, showing excellent agreement in the intermediate range, 500–1000 K. Both theories show good agreement with each other in the common temperature range, 300–2000 K, with differences from 3% at 300 K to 25% at 2000 K. Because both theories use the same PES-2020 surface, this agreement is a new test of consistency of the functional form describing this polyatomic system. It is known that the RPMD theory is exact at the high temperature limit [12] and therefore, these results show that the CVT/μOMT overestimate the rate constant by only 25%, which represents an excellent result given the approaches used in TST-based methods [37, 38], mainly the choice of the dividing surface between reactants and products at a point $s^*(T)$, which is related with recrossing effects, and with the treatment of the anharmonicity [39]. With respect to the low temperature regime, it is known that RPMD theory overestimates the tunnelling contribution in asymmetric reactions [21, 24], by a factor of up to 4 in the less favorable conditions. However, interestingly, this strong overestimation is not found in the present study.

Six years ago, we performed a comparative study of the VTST/MT and RPMD theories using the "cousin" $O(^3P) + CH_4$ reaction [20] based on an accurate full-dimensional PES describing this polyatomic system [40], named PES-2014, at the temperature range 200–2500 K. This reaction and the title reaction present a similar topology from reactants to products. So, both reactions present a similar classical reaction energy, 5.8 vs 2.22 kcal mol^{-1} and a high barrier, 14.1 vs 10.70 kcal mol^{-1}. In the former study, we also found a good agreement between both theories and of these ones with experimental values. So, at high temperatures, while RPMD theory simulates perfectly the experimental rate constants, the VTST/MT results are smaller, and at low temperatures, when the tunnelling contribution plays an important role, both methods slightly overestimated the experimental rate constants. Therefore, both theories capture the recrossing effects at high temperatures and the tunnelling factor at low temperatures, both in the $O(^3P) + CH_4$ and in the $O(^3P) + C_2H_6$ reactions. The discrepancies with the experimental measurements may be due to several factors: deficiencies of the surfaces (PES-2014 and PES-2020), and limitations of the theories used (VTST/MT and RPMD), without forgetting uncertainties in the experimental data reported.

Finally, on many occasions we can find in the literature that QCT calculations are used in kinetics studies, in spite of its classical nature. The QCT rate constants on the PES-2020 surface at selected temperatures also appear in Table 2 and Fig. 3, using two approaches: by considering all reactive trajectories (QCT-all) and by discarding those reactive trajectories that do not meet the DZPE criterium (QCT-DZPE). In this case, with both approaches, the behavior is very different at low and high temperatures. While at high temperatures, 1000–2000 K, the agreement with experiments is reasonable, better than with Tsang-Hampson's review of 1986 [8], at low temperatures both QCT approaches differ greatly from experiments and VTST/MT or RPMD theories, despite the fact that tunnelling factor is included in the QCT rate constant by multiplying it by the tunnelling correction obtained in the VTST/MT theory. When the tunnelling factor is not included in CVT/μOMT and QCT/μOMT rate constants, i.e., in the CVT vs QCT comparison, the differences are, obviously, the same. So, at 300 K the rate constants are, respectively, 1.44×10^{-16} versus 5.45×10^{-15} (both for QCT-all and QCT-DZPE approaches), while at 1000 K, the values are $2.84.10^{-12}$ versus 2.87×10^{-12} (1.86×10^{-12} with DZPE correction). At this moment, is unclear the reason of this strong discrepancy at low temperatures, given that the same tunnelling factor is applied in both theories. A possible explanation is that at 300 K the reactivity is very reduced given the high barrier of reaction, 10.70 kcal mol^{-1}. For instance, at 300 K, of the 500,000 trajectories run in QCT calculations, only 55 were reactive, i.e., 0.011%. This represents a reaction cross section of 7.77×10^{-4} $Å^2$, and an uncertainty of 13%. In addition, it is surprising that at low temperature both QCT-all and QCT-DZPE methods give the same rate constant, i.e., no ZPE violation is found. At this moment, we do not have a clear explanation for this behavior. Therefore, for the title reaction, the QCT approach is not a good alternative for the kinetics study, especially at low temperatures.

4 Activation energy and kinetic isotope effects

Other kinetics properties, such as activation energy or kinetics isotope effects (KIE), have not been previously reported. So, the results from the present study have a predictive character, to be confirmed or not by future studies, theoretical or experimental. Note that given the high computational cost of the RPMD calculations as compared to the VTST/MT approach, and the good agreement between both theories, in this section the VTST/MT results will be used (unless otherwise stated) based on the PES-2020 surface.

While the classical barrier height, $\Delta E^{\neq}$, represents an interesting theoretical magnitude on the topology of the reaction, the activation energy (which includes temperature and other thermochemical magnitudes) represents a property that is more directly related with experimental measurements. Table 3 lists the activation energy at different temperature ranges. As in the case of the rate constants (Fig. 3), the theoretical activation energies are intermediate between the two experimental reviews [8, 9] used for comparison.

Table 3 Activation energy (kcal mol^{-1}) for the title reaction using CVT/μOMT theory on the PES-2020 surface at different temperatures

T(K)	300–500	500–1000	1000–1500	1500–2000
This work	6.18	8.17	10.68	12.82
Exp-1986[a]	7.77	8.14	8.75	9.37
Exp-1991[b]	5.22	9.23	12.42	13.96

[a]Experimental values from Ref. [8], obtained from the slope of the plot in Fig. 3

[b]Experimental values from Ref. [9], obtained from the slope of the plot in Fig. 3

Table 4 H/D and $^{12}C/^{13}C$ kinetic isotope effects at different temperatures for the $O(^3P)+C_2H_6$ and isotope variant reactions. The KIEs for the "cousin" $O(^3P)+CH_4$ reactions are also included

T (K)	$O(^3P)+C_2H_6$[a]		$O(^3P)+CH_4$[b]	
	R1/R2	R1/R3	R1/R2	R1/R3
200	46.55	0.98 (0.95)	136.66	1.03
300	13.80	0.94 (0.99)	18.64	1.03
500	4.55	1.48 (1.02) [1.02]	3.44	1.03
1000	1.87	1.19 (0.95) [1.04]	1.43	1.02
1500	1.42	1.05 (1.06)	1.40	1.02
2000	1.25	0.91 (1.00)	1.25	1.02
3000	1.18	0.90 (1.00)		

[a]For the $O(^3P)+C_2H_6$ reactions, the CVT/μOMT rate constants on the PES-2020 surface are used, as obtained in the present study. In parentheses, R1/R3 KIEs using anharmonic corrections (see text). In brackets, R1/R3 KIEs using the RPMD theory

[b]The KIEs for the $O(^3P)+CH_4$ reactions are obtained from Ref. 20, and they were calculated from CUS/LAT rate constants on the PES-2014 surface. CUS means canonical unified statistical model, and LAT represents the least-action tunnelling method. See original paper, Ref. [20], for more details. Note that in that paper, only the R1/R2 KIEs were reported

Another interesting kinetics property from the mechanistic point of view is the kinetic isotope effect, KIE. Because KIEs depend on the masses of reactants, they are a good candidate for testing quantum effects in the reaction, tunnelling and ZPE. The VTST/MT KIEs at different temperatures are listed in Table 4 and they are defined as the ratio between the rate constants from the lighter to the heavier isotope. The following isotope reactions were considered:

$$O(^3P) + C_2H_6/CH_4 \rightarrow OH + C_2H_5/CH_3 \quad \text{(R1)}$$

$$O(^3P) + C_2D_6/CD_4 \rightarrow OD + C_2D_5/CD_3 \quad \text{(R2)}$$

$$O(^3P) + {}^{13}C_2H_6/{}^{13}CH_4 \rightarrow OH + {}^{13}C_2H_5/{}^{13}CH_3 \quad \text{(R3)}$$

In the case of the title reaction, for the deuterated reaction, R1/R2, the KIEs monotonically decrease with temperature, from 46.55 at 200 K to 1.18 at 3000 K. However, the behavior of the $^{12}C/^{13}C$ KIEs is different, increasing up to 500 K, and after decreasing with temperature with values close to unity (except at intermediate temperatures). Unfortunately, neither experimental nor theoretical data are available for comparison. Therefore, here we use the "cousin" $O(^3P)+CH_4$ reaction for comparison [20], and the KIEs are also included in Table 4, where as far as we know experimental information is not available either. Both reactions follow a similar tendency with temperature, both for the R1/R2 KIEs (decreasing with temperature) and for the R1/R3 KIEs (with values close to unity). We expect that these results will be interesting for experimentalists and incentive future researches.

In order to understand this behavior with temperature for the title reaction, a factorization analysis was performed, where the KIE(T) was separated in three components: zero-point energy (ZPE), recrossing and tunnelling. The first one is related with the adiabatic barrier height for each isotope, $\Delta H^{\neq}(0\ K)$. Given that the classical barrier height, $\Delta E^{\neq}$, is the same for all isotopes, it measures the influence of the vibrational frequencies due to the ZPE corrections. It is defined as the ratio of conventional TST($s=0$) rate constants for each isotope, $\text{ZPE} = k^{\text{TST}}(^{12}C_2H_6)/k^{\text{TST}}(^{12}C_2D_6 \text{ or } ^{13}C_2H_6)$. In fact, the ZPE component also includes the change of the rotational partition function due to the change of masses and the change of the vibrational partition function in $\Delta G^{\text{GT,o}}$. The second one is related with variational effects and represents the ratio between KIEs calculated using variational and conventional TST theories, $\text{Recrossing} = \text{KIE}^{\text{CVT}}/\text{KIE}^{\text{TST}}$. Finally, the third one is the ratio of tunnelling factors, $\text{Tunneling} = \kappa^{\mu\text{OMT}}(^{12}C_2H_6)/\kappa^{\mu\text{OMT}}(^{12}C_2D_6 \text{ or } ^{13}C_2H_6)$, and as is obvious, it measures the tunnelling contribution. The factorization analysis for the $O(^3P)+C_2H_6$ reaction is shown in Table 5. The large KIEs for the H/D, R1/R2, reactions, are due mainly to the effect of the ZPE in the barrier height, $\Delta H^{\neq}(0\ K) = 6.78$ versus 8.06 kcal mol^{-1}, respectively, for the H and D reactions, i.e., the ZPE contribution diminishes the barrier for the perprotio reaction more than for the deuterated one. The second factor in importance is tunnelling, where the H transfer is favoured on the D transfer. The recrossing effect is small, and all three factors diminish with temperature. The KIEs for the $^{12}C/^{13}C$, R1/R3, reactions are close to unity (Table 4) and are due to a compromise between the three factors analyzed, all close to unity. The tunnelling and ZPE factors are small, in the first case because the same H atom is transferred, and in the second case because both isotopes present similar adiabatic barrier height, $\Delta H^{\neq}(0\ K) = 6.78$ versus 6.80 kcal mol^{-1}. It is now observed that the peak at intermediate temperatures (Table 4) is due to recrossing effects, which are strongly dependent on the choice of dividing surface and it is related with the harmonic/anharmonic treatment of the lowest

Table 5 Kinetic isotope effects factor analysis for the $O(^3P)+C_2H_6$ reaction at different temperatures

T (K)	R1/R2			R1/R3		
	ZPE	Recrossing	Tunnelling	ZPE	Recrossing	Tunnelling
200	8.96	1.35	3.84	1.00	0.90	1.09
300	4.48	1.43	2.16	1.03	0.87	1.06
500	2.46	1.36	1.36	1.05	1.37	1.03
1000	1.59	1.09	1.08	1.07	1.11	1.01
1500	1.43	0.96	1.04	1.07	0.98	1.00
2000	1.38	0.89	1.02	1.07	0.85	1.00
3000	1.36	0.86	1.01	1.08	0.84	1.00

vibrational frequencies along the reaction path or the mode-mode coupling, a limitation of the TST-based theories, as previously noted.

Finally, in order to study this possibility, we have analyzed in detail the importance of the anharmonicity on the final $^{12}C/^{13}C$ KIEs, R1/R3. However, the anharmonic calculation is not straightforward in polyatomic reactions. To the best of our knowledge, in these cases no general methods have been proposed to deal (successfully) with anharmonicity along the reaction path. While the calculation of anharmonic vibrations at stationary points is affordable, the calculation at non-stationary points (i.e. points along the reaction path) is not straightforward. The problem is how to project out from the Hessian matrix the motion in the direction of the reaction path. Unfortunately, in the POLYRATE code the anharmonicity calculation is not included when large curvature tunnelling methods are used. Therefore, this analysis is necessarily qualitative. In a similar way as in a previous study on the $O(^3P)+CH_4$ reaction [20], we qualitatively analyzed this problem using the WKB (Wentzel-Kramers-Brillouin) approximation applied on the reactive mode, C–H–O, which is a symmetric stretching mode related with the hydrogen transfer. Note that in its present implementation only the vibrational ground state is used in this approach, while harmonic approximations are used in the calculation of higher vibrational levels. The anharmonic $^{12}C/^{13}C$ KIEs are also included in Table 4. Clearly, the overestimation of the KIEs at intermediate temperatures disappears and now all KIEs in the wide temperature range, 200–3000 K, are close to unity. Therefore, although the analysis is qualitative, we have shown the importance of the anharmonicity on this property. Next, we analyze this problem from other point of view, using the RPMD theory. As noted previously, RPMD is immune to the location of the dividing surface between reactants and products and, consequently, to the problem of anharmonicity previously reported. Table 4 also includes the $^{12}C/^{13}C$ KIEs at 500 and 1000 K using the RPMD theory (for the ^{13}C isotope we use the same RPMD parameters as reported in Table 1). The KIEs are, respectively, 1.02 and 1.04 and, therefore, the overestimation obtained with the VTST theory disappears. We conclude that the $^{12}C/^{13}C$ KIEs are close to unity and practically independent on temperature in the 200–3000 K temperature range.

5 Conclusions

The kinetics (thermal rate constants and kinetic isotope effects) of the $O(^3P)+C_2H_6$ hydrogen abstraction gas-phase reaction was analyzed using three theoretical tools: VTST/MT, RPMD and QCT, where all studies are based on an analytical full-dimensional surface, PES-2020. The QCT calculations, given their classical nature, failed in the description of the rate constants at low temperatures, with differences of a factor of about 20 at 300 K with respect to experiments. VTST/MT and RPMD rate constants agree with each other in the common temperature range, 300–2000 K, with differences of less than 25%, and they simulate the experimental evidence, with a non-Arrhenius behavior. This good agreement shows that both theories capture the zero-point energy contribution, the tunnelling effects at low temperatures and the recrossing effects at high temperatures. These findings contrast with the behavior observed in the "cousin" $O(^3P)+CH_4$ hydrogen abstraction reaction previously analyzed in our group [20]. There, while at low temperatures both theories agree between them, though overestimating the experimental information, at the higher temperature regime, where the RPMD is exact, they differ by a factor of 2.

Due to its cheaper computational cost, the kinetic isotope effects, KIEs, were analyzed using the VTST/MT theory for the H/D and $^{12}C/^{13}C$ isotopes in the temperature range 200–3000 K and, unfortunately, no experimental data are available for comparison. For the H/D isotopes, the KIEs present large values, decreasing with temperature. This behavior is related with the fact that the adiabatic barrier at 0 K for the perprotio reaction is lower than for the deuterated one, 6.78 versus 8.06 kcal mol^{-1}, ZPE factor, and with the larger tunnelling contribution for the lighter isotope (H) at low temperatures (tunneling factor). For the $^{12}C/^{13}C$ isotopes, the KIEs are close to unity, and this value is due to a cancellation of the ZPE, tunnelling and recrossing factors,

all of them near to unity. The behavior for both H/D and $^{12}C/^{13}C$ KIEs for the title reaction is similar to that found for the $O(^3P) + CH_4$ reaction.

After a complete theoretical study on the title reaction, *ab initio* electronic structure calculations and dynamics study in a previous paper [3] and kinetics study in the present work, where good agreement is found with many kinetics and dynamics experimental measures, we conclude that PES-2020 is accurate and adequate to study this nine-body polyatomic system.

Acknowledgements This work was partially supported by Junta de Extremadura and European Regional Development Fund, Spain (Projects Nos. GR18010 and IB16013).

References

1. Warnatz J, Gardiner WC (eds) (1984) Combustion chemistry. Springer-Verlag, New York
2. NIST Chemical Kinetics Database web page. Standard Reference Database 17, Version 7.0 (web version), Release 1.6.8. Data version 2015.09
3. Espinosa-Garcia J, Rangel C, Corchado JC, Garcia-Chamorro M (2020) Phys Chem Chem Phys 22:22591
4. Mayer SW, Schieler L (1968) J Phys Chem 72:2628
5. Mahmud K, Marshall P, Fontijn A (1988) J Chem Phys 88:2393
6. Troya D (2007) J Phys Chem A 111:10745
7. Huynh LK, Zhang S, Truong TN (2008) Combust Flame 152:177
8. Tsang W, Hampson RF (1986) J Phys Chem Ref Data 15:1087
9. Cohen N, Westberg KR (1991) Int J Chem Kinet 18:990
10. Fernandez-Ramos A, Ellingson BA, Meana-Pañeda R, Marques JMC, Truhlar DG (2007) Theor Chem Acc 118:813
11. Liu Y-P, Lu Dh, Gonzalez-Lafont A, Truhlar DG, Garrett BC (1993) J Am Chem Soc 115:7806
12. Zheng J et al (2016) POLYRATE-2016-2A. University of Minnesota, Minneapolis
13. Suleimanov YV, Collepardo-Guevara R, Manolopoulos DE (2011) J Chem Phys 134:044131
14. Gillan MJ (1987) Phys Rev Lett 58:563
15. Gillan MJ (1987) J Phys C Solid State Phys 20:3621
16. Voth GA, Chandler D, Miller WH (1989) J Chem Phys 91:7749
17. Suleimanov YV, Allen JW, Green WH (2013) Compu Phys Commun 184:833
18. Tudela RP, Aoiz FJ, Suleimanov YV, Manolopoulos DE (2012) J Phys Chem Lett 3:493
19. Allen JW, Green WH, Li Y, Guo H, Suleimanov YV (2013) J Chem Phys 138:221103
20. Gonzalez-Lavado E, Corchado JC, Suleimanov YV, Green WH, Espinosa-Garcia J (2014) J Phys Chem A 118:3243
21. Suleimanov YV, Kong WJ, Guo H, Green WH (2014) J Chem Phys 141:244103
22. Suleimanov YV, Espinosa-Garcia J (2016) J Phys Chem B 120:1418
23. Novikov IS, Shapeev AV, Suleimanov YV (2019) J Chem Phys 151:224105
24. Espinosa-Garcia J, Gacia-Chamorro M, Corchado JC, Bhowmick S, Suleimanov YV (2020) Phys Chem Chem Phys 22:13790
25. Richardson JO, Althorpe SC (2009) J Chem Phys 131:214106
26. Nyman G, Davisson J (1990) J Chem Phys 92:2415
27. Varandas AJC, Marques JMC (1992) J Chem Phys 97:4050
28. Varandas AJC (1993) J Chem Phys 99:1076
29. Nyman G (1993) Chem Phys 173:159
30. Varandas AJC (1994) Chem Phys Lett 225:18
31. Hu X, Hase WL, Pirraglia T (1991) J Comput Chem 12:1014
32. Hase WL et al (1996) VENUS96: a general chemical dynamics computer program. QCPE Bull 16:43
33. Ausfelder F, McKendrick KG (2000) Progress in reaction kinetics and mechanism. Sci Technol Lett 25:299–370
34. Sweeney GM, Watson A, McKendrick KG (1997) J Chem Phys 106:9172
35. Sweeney GM, Watson A, McKendrick KG (1997) J Chem Phys 106:9182
36. Troya D, Pascual R, Garton DJ, Minton TK, Schatz GC (2003) J Phys Chem A 107:7161
37. Klippenstein SJ, Allen WD (1997) Ber Bunsen-Ges Phys Chem 101:423
38. Li Y, Suleimanov YV, Guo H (2014) J Phys Chem Lett 5:700
39. Sanson JA, Sanchez ML, Corchado JC (2006) J Phys Chem A 110:589
40. Gonzalez-Lavado E, Corchado JC, Espinosa-Garcia J (2014) J Chem Phys 140:064310